

A discontinuous control volume finite element method for multi-phase flow in heterogeneous porous media

P. Salinas ^{a,b,*}, D. Pavlidis ^{a,b}, Z. Xie ^c, H. Osman ^{a,b}, C.C. Pain ^{a,b}, M.D. Jackson ^b

^a Applied Modelling and Computation Group, Department of Earth Science and Engineering, Imperial College London, UK

^b Novel Reservoir Modelling and Simulation Group, Department of Earth Science and Engineering, Imperial College London, UK

^c Now at School of Engineering, Cardiff University, Cardiff, CF24 3AA, UK

ARTICLE INFO

Article history:

Received 24 November 2016

Received in revised form 26 June 2017

Accepted 29 September 2017

Keywords:

CVFEM mixed formulation

Discontinuous Galerkin

Multiphase flows

Porous media

ABSTRACT

We present a new, high-order, control-volume-finite-element (CVFE) method for multi-phase porous media flow with discontinuous 1st-order representation for pressure and discontinuous 2nd-order representation for velocity. The method has been implemented using unstructured tetrahedral meshes to discretize space. The method locally and globally conserves mass. However, unlike conventional CVFE formulations, the method presented here does not require the use of control volumes (CVs) that span the boundaries between domains with differing material properties. We demonstrate that the approach accurately preserves discontinuous saturation changes caused by permeability variations across such boundaries, allowing efficient simulation of flow in highly heterogeneous models. Moreover, accurate solutions are obtained at significantly lower computational cost than using conventional CVFE methods. We resolve a long-standing problem associated with the use of classical CVFE methods to model flow in highly heterogeneous porous media.

© 2017 The Author(s). Published by Elsevier Inc. This is an open access article under the CC BY license (<http://creativecommons.org/licenses/by/4.0/>).

1. Introduction

Many geologic porous media are highly heterogeneous: they contain domains of contrasting material properties such as porosity, permeability and capillary pressure. Moreover, these domains often have complex three dimensional (3D) geometries and spatial distribution, and the changes in material properties across the domain boundaries are effectively discontinuous, because they occur over a few tens or hundreds of grains (e.g. [24], [12], [44], [38], [27], Fig. 1).

Classical approaches for modelling multiphase flow in porous media use finite differences (FD) for structured meshes and finite volumes for unstructured meshes (e.g. [47], [4], [13]). However, most implementations use the two-point flux approximation (TPFA) to compute the fluxes between cells which is correct only if the mesh is k-orthogonal. This places significant limitations on the geometry of the mesh used to discretize heterogeneous porous media (e.g. [28], [41], [54]). Alternatives have been developed to overcome this problem, such as the multi-point flux approximation (e.g. [1], [45], [46], [56], [6]).

An alternative to FD and FV methods is the use of finite elements (FE) together with control volumes (CV), known as the control volume finite element (CVFE) method. Research into the CVFE method for porous media flow dates back to the 1970s (e.g. [35], [11], [22], [23], [17], [18], [30], [5], [19], [24], [53], [33], [40], [39], [50], [36], [43], [42], [49]). This approach combines the flexibility of finite-element discretizations that are well suited to capture complex geologic

* Corresponding author at: Applied Modelling and Computation Group, Department of Earth Science and Engineering, Imperial College London, UK.
E-mail address: pablo.salinas@imperial.ac.uk (P. Salinas).

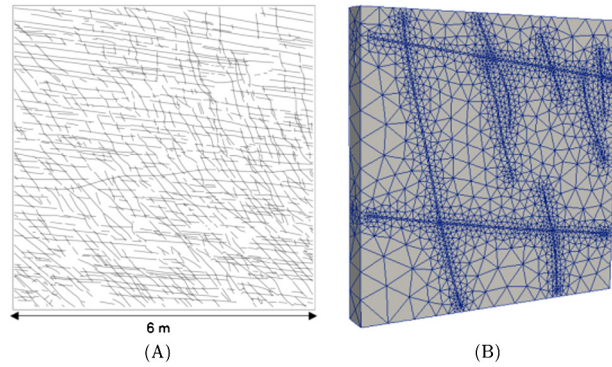


Fig. 1. Example of heterogeneous geology with domains of contrasting properties. (A) Planview of fractures with high permeability (shown as gray lines) embedded within porous matrix of low permeability (shown in white). Example from [8]. (B) Model of part of (A) using parametric surfaces to represent the fractures, showing also the unstructured tetrahedral mesh used to discretize space.

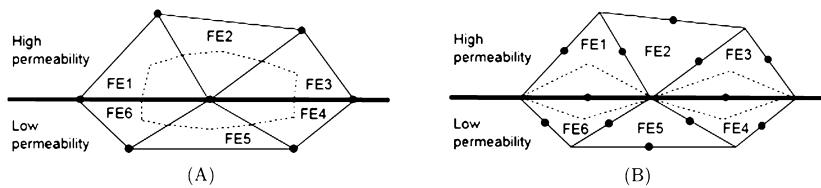


Fig. 2. (A) Conventional CVFE representation in which control volumes (CVs) are formed around pressure nodes and saturation is represented CV-wise. Finite elements (FEs) (1), (2) and (3) lie within a high permeability domain; FEs (4), (5) and (6) lie within a low permeability domain. If the phase saturation in the high permeability domain changes, the saturation change spreads artificially into the low permeability domain via the shared CV. (B) Face-centred CV formulation implemented by [2]. Each CV is shared across at most two FEs so the spreading of saturation from the high into the low permeability domain is reduced, but not eliminated.

architectures (e.g. Fig. 1), with the capabilities of control-volume methods to produce stable, locally mass-conservative solutions ([50]). Typically, pressure and velocity, and material properties, such as permeability and porosity, are represented FE-wise, but mass conservative properties such as saturation and concentration are represented CV-wise.

In standard CVFE methods, the CVs span the boundaries between contrasting material properties (Fig. 2(A)). This creates a problem when there are contrasts in permeability or capillary entry pressure across the boundary. A number of studies have considered the case of contrasting capillary entry pressure, where appropriate conditions need to be implemented at the boundary to ensure the correct physical representation (see [15], [16], [31], [32] and [14]). Here, we focus on the geologically common situation in which there are significant permeability contrasts across the boundary. In this case, the use of CVs that span the boundary causes mass to artificially leak out of high permeability domains and into low (or zero) permeability domains and vice-versa (e.g. [7], [44], [2], [52], Fig. 1(B)). Fluid saturation and component concentration are therefore smeared across neighbouring elements ([2]). This issue has led some authors to argue that, despite the advantages outlined above, CVFE methods are not suitable for modelling multiphase flow in highly heterogeneous porous media (e.g. [21], Fig. 2(A)).

Several recent papers have addressed the problem of CVs that span domain boundaries in heterogeneous porous media. [44] separated the CVs at FE interfaces that correspond to domain boundaries, and employed the average flux between elements at the interface. However, this approach does not guarantee local mass conservation. [7] used the boundary FEs as CVs and enforced mass conservation in a post-processing step to calculate the fluxes between CVs. However, this approach is numerically expensive and inconsistent, and was also tested on 2D elements with a radial construction of the local mass conservation equations, which is not the case in general 3D elements. [2] constructed CVs around FE boundaries rather than FE nodes, which reduces the ‘smearing’ because each CV spans at most two FEs (Fig. 2(B)). However, the approach is numerically expensive, as the number of degrees of freedom at FE interfaces can be more than nine times the number of degrees of freedom at FE nodes in a tetrahedral mesh. Furthermore, the smearing effect is not eliminated, as CVs still span more than one FE. Thus, higher mesh resolution is still required at domain boundaries to reduce the ‘smearing’ effect. [52] introduced a new element pair which eliminates the ‘smearing’ effect by employing CVs that are discontinuous between FEs. The method is numerically consistent because pressure is also discontinuous. Their results were promising, but the method was implemented only in 2D. Most models of interest in porous media flow are 3D.

The first key aim of this paper is to develop and implement a new CVFE method in 3D that does not require the use of control volumes (CVs) that span domain boundaries in heterogeneous porous media. We implement discontinuous CVs here by allowing pressure to be discontinuous between elements, using the element pair first presented by [52] which has a discontinuous 1st-order representation for pressure, and a discontinuous 2nd-order representation for velocity. The (discontinuous) pressure and velocity fields are solved using a FE approach and saturation is updated within CVs, but the CVs do

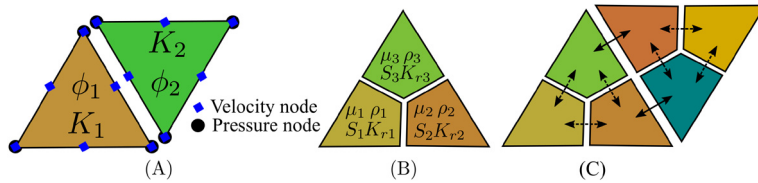


Fig. 3. (A) 2D representation of a P_2 DG– P_1 DG element pair. Porosity ϕ and permeability \mathbf{K} are piecewise constant within FEs. The velocity nodes are associated to the element corners and the mid-points of the element edges; pressure nodes are associated to the corners of the elements. (B) The three CVs that fit into a 2D element. Saturation and saturation-dependent variables are piecewise constant within CVs. (C) Fluxes calculated within and between FEs. Dashed arrows denote fluxes across CV boundaries within a FE; filled arrows denote fluxes across CV and FE element boundaries.

not span adjacent elements. The method conserves mass. The second key aim is to demonstrate that for very heterogeneous domains this new formulation requires fewer degrees of freedom than classical CVFE methods. We demonstrate that the approach, amongst other features, accurately preserves sharp saturation changes associated with significant permeability contrasts across high aspect ratio geologic features such as fractures and thin mudstones, allowing efficient simulation of flow in highly heterogeneous models.

2. Numerical method

The method developed is applicable to N_p fluid phases and to the general family of P_{n+1} DG– P_n DG element pairs, where P denotes the polynomial approximation to the solution field, n denotes the order of the polynomial approximation and DG denotes Discontinuous Galerkin. However, for brevity and clarity we describe here only the implementation for two phases (a wetting phase w and a non-wetting phase nw) and for the element pair, in which pressure varies linearly across elements and is discontinuous between elements, and velocity has a quadratic variation across elements and is also discontinuous between elements. The discontinuous pressure, a key difference to other CVFE methods reported previously, allows the use of CVs that do not span multiple FEs; rather, each CV here is associated with a single FE, Fig. 3. Saturation, and all saturation-dependent material properties such as relative permeability are represented CV-wise; the remaining material properties, such as porosity and permeability, are represented FE-wise. For simplicity, Fig. 3(A) shows this for a 2D (triangular) element; the formulation described is equivalent for 3D (tetrahedral) elements. Hence each CV (and FE) is associated with a unique set of petrophysical properties. All the numerical methods reported here are implemented within a single, integrated open-source code, available under the terms of the Lesser General Purpose License (LGPL): the Imperial College Finite Element Reservoir Simulator (IC-FERST). Further information about the code can be found in [36], [26] and [55].

For simplicity and following the approach of [36] we assume rock and fluids are incompressible and write the mass balance equation for phase p as

$$\varphi \frac{\partial S_p}{\partial t} + \nabla \cdot (\mathbf{v}_p S_p) = q_p, \quad (1)$$

where φ represents the porosity, $p \in [1, N_p]$ represents the phase, S is saturation, \mathbf{v} is the saturation-weighted Darcy velocity (such that $\mathbf{v}_p S_p$ is the traditional Darcy velocity of phase p). The velocity is defined this way in order to reduce the non-linearity of the problem: relative permeability is often a power-law function of saturation (or similar), so dividing through by saturation has the effect of reducing the non-linearity. Finally, q is a volume source term, subject to the constraint on saturation

$$\sum_{p=1}^{N_p} S_p = 1, \quad \forall N_p. \quad (2)$$

Incompressibility is not an essential assumption but applies to all the examples shown here. We write Darcy's law for a generic phase p as:

$$\left(\frac{S_p \mu_p}{k_{r_p}} \right) \mathbf{K}^{-1} \mathbf{v}_p = \sigma_p \mathbf{v}_p = -\nabla P + \rho_p \mathbf{g}, \quad (3)$$

where S , \mathbf{K} , k_r and μ are saturation, permeability tensor, relative permeability and viscosity respectively, ρ is the density, \mathbf{g} is the acceleration due to gravity acting in the vertical direction and P is the fluid phase pressure. By analogy with the Navier–Stokes equation and consistent with [36], we treat σ as an absorption term, with coupled FE and CV representation of the nonlinear convolution of saturation, relative permeability and permeability tensor fields which is piecewise constant within each FE and CV; the permeability tensor is defined with respect to the global model coordinate system and may be locally rotated to align with bedding and other geologic heterogeneities interpreted to be present in a given geologic domain.

Eq. (1) is discretized in time and space following the approach of [36] in which the time discretization is obtained using the θ -method, which smoothly switches from Crank–Nicolson (CN) to backward-Euler (BE) methods (see [9], as implemented by [25]), and the space discretization is obtained by testing the weak form of the equation over each CV using lagrangian CV basis functions M_i . Summing over all phases and discretizing in time using the θ -method yields the discretized form of the global mass balance equation defined in CV space

$$\sum_{p=1}^{\mathcal{N}_p} \int_{\Omega_{CV_i}} M_i \left(\frac{\varphi(S_{pi}^{n+1} - S_{pi}^n)}{\delta t} dV \right) - \int_{\Gamma_{CV_i}} M_i q_{pi}^{n+\theta} dV + \int_{\Gamma_{CV_i}} \left(\theta^{n+\frac{1}{2}} \mathbf{n} \cdot \mathbf{v}_{pi}^{n+1} S_{pi}^{n+1} + (1 - \theta^{n+\frac{1}{2}}) \mathbf{n} \mathbf{v}_{pi}^n S_{pi}^n \right) d\Gamma, \tag{4}$$

where Ω_{CV_i} and Γ_{CV_i} are the volume and boundary of CV i respectively, \mathbf{n} is the normal vector of the CV, \mathbf{v}_{pi} is the saturation-weighted velocity of phase p projected onto the CV boundary, and θ varies smoothly between 0.5 (corresponding to CN) and 1 (corresponding to BE) to avoid the introduction of spurious oscillations for large grid Courant numbers. Eq. (4) can be expressed in matrix form at time level $n + 1$ as

$$B \underline{\mathbf{v}}^{n+1} = \underline{\mathbf{q}}^{n+1} \tag{5}$$

where $\underline{\mathbf{v}}$ is the vector of discretized saturation-weighted Darcy velocities projected onto the CV boundaries. The multiphase Darcy law Eq. (3) is also discretized following the approach of [36], by defining standard basis functions for pressure and velocity and testing with the velocity basis function space, except here we need to account for the discontinuity in pressure as well as velocity between elements. Thus, we integrate Eq. (3) by parts twice, in order to add the term that accounts for the discontinuous pressure, yielding

$$\sum_{E_j} \int_{\Omega_{E_j}} Q_j (\boldsymbol{\sigma}_p \mathbf{v}_p + \nabla P_p - \rho_p \mathbf{g}) dV + 0.5 \int_{\Gamma_{E_j}} Q_j \mathbf{n} (P_p - P_{p_{nab}}) d\Gamma + \int_{\Gamma_{\Omega}} Q_j \mathbf{n} (P_p - P_{p_{bc}}) d\Gamma = \mathbf{0}, \tag{6}$$

where Ω_{E_j} and Γ_{E_j} are the volume and boundary of element j respectively, P and \mathbf{v} are the element-wise pressure and saturation-weighted Darcy velocity respectively, Γ_{Ω} is the model boundary, P_{bc} are pressure boundary conditions (if specified), Q_j are Lagrangian velocity basis functions and \mathbf{n} is the normal to the element. P_{nab} is the pressure of the neighbouring node that shares the same spatial coordinates as the node containing the value of P , Fig. 3 (A); terms containing this vanish if pressure is continuous, yielding the formulation presented by [36].

Pressure and velocity are expressed in terms of their FE lagrangian basis functions Q_j and L_j , respectively, as:

$$\mathbf{v}_p = \sum_{j=1}^{\mathcal{N}_u} Q_j \mathbf{v}_{p,j} \quad \text{and} \quad P = \sum_{j=1}^{\mathcal{N}_p} L_j P_j. \tag{7}$$

Here \mathcal{N}_u and \mathcal{N}_p are the total number of degrees of freedom for the FE force and pressure representations.

Eq. (6) can be expressed in matrix form at time level $n + 1$ as

$$M_{\sigma} \underline{\mathbf{v}}^{n+1} = -C \underline{\mathbf{P}}^{n+1} - \underline{\Lambda}^{n+1} \tag{8}$$

Pressure is obtained by combining Eqs. (5) and (8) to eliminate the velocity, yielding

$$B M_{\sigma}^{-1} C \underline{\mathbf{P}}^{n+1} = B M_{\sigma}^{-1} \underline{\Lambda}^{n+1} - \underline{\mathbf{q}}^{n+1}. \tag{9}$$

After the pressure is obtained, the velocity is obtained using Eq. (8) and then the saturation field is calculated using Eq. (5) subject to the constraint of Eq. (2).

The implementation of discontinuous pressure requires a new approach to calculating fluxes between CVs. For formulations with CVs that span multiple elements, the interface between different CVs is located within the FEs. However, in the formulation presented here, interfaces are located both inside and between FEs. Inside FEs, we determine interface fluxes (shown by dashed arrows in Fig. 3 (C)) using the same procedure as [36]: a flux-limited interface absorption term is calculated using the CV-wise values of σ on either side of the interface. Between FEs, we determine interface fluxes (shown by the solid arrows in Fig. 3 (C)) using a weighted average given by

$$\hat{v}_p = (\Omega_{nab} \sigma_{p_{nab}} \mathbf{v}_{p_{cur}} + \Omega_{cur} \sigma_{p_{cur}} \mathbf{v}_{p_{nab}}) (\Omega_{nab} \sigma_{p_{nab}} + \Omega_{cur} \sigma_{p_{cur}})^{-1}, \tag{10}$$

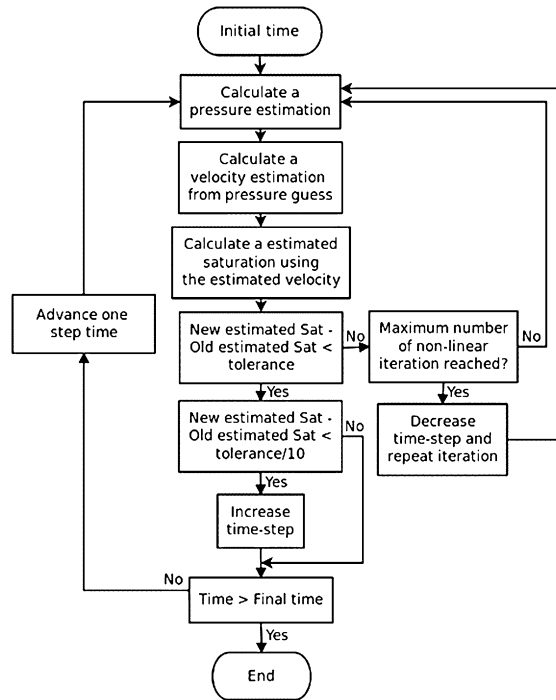


Fig. 4. Flow chart showing the solution steps. There are two main loops. One is the fixed-point iteration method, which is used to solve the non-linear system of equations; the other is the time-stepping loop.

where the subscript *nab* denotes the neighbouring node and *cur* denotes the current node. Note that flux continuity is enforced across CVs. For CVs with boundaries within a given FE the flux is simple mapped from the FE; for CVs that span with interfaces between FEs, flux continuity is enforced by Eq. (10). Thus local mass conservation is guaranteed.

To solve the non-linear system of equations, Eq. (5), Eq. (8) and Eq. (9) (where the non-linearity arises primarily from the relative permeability), we use an Anderson-fixed-point iteration method ([3]), this allows us to solve the system of equations directly. A description and analysis of the convergence of this non-linear solver is reported in [48]. Only a brief overview is provided here, as the new space discretization we report does not depend directly on the chosen solution method. We first obtain an estimated pressure solution, then an estimated velocity, and finally an estimated saturation. We iterate until a certain pre-defined saturation tolerance is reached, in which case the size of the next time-step is increased, or until a pre-determined maximum number of non-linear iterations is reached, in which case the current time-step is decreased (Fig. 4). We choose these convergence limits because the main non-linearity appears in the saturation equation (e.g. [37]) and control of the residual may fail if the solution is too flat (e.g. [51]). The chosen criteria work well in all of the example cases shown. As the focus of this paper is the new discretization method, we limit the maximum number of fixed-point iterations to 3, but this is not a limitation of the methodology; nor is it required.

3. Numerical experiments

We test the formulation using a number of two and three-dimensional (2-D and 3-D) models. In these the relative permeability of each phase is given by

$$k_{rw}(S_w) = \left(\frac{S_w - S_{wirr}}{1 - S_{wirr} - S_{nwr}} \right)^{n_w}, \tag{11}$$

$$k_{rnw}(S_w) = \left(\frac{S_{nw} - S_{nwr}}{1 - S_{wirr} - S_{nwr}} \right)^{n_{nw}}, \tag{12}$$

where S_{wirr} and S_{nwr} are the immobile fractions of the wetting and non-wetting phase respectively.

The properties of the models are summarized in Table 1. In all models, unless otherwise stated, the outlet boundary has a dimensionless pressure of 0, the models are initially saturated with the non-wetting phase and the wetting phase at the irreducible saturation, and the wetting phase is injected over the inlet boundary with a dimensionless velocity of 1. Dimensionless time is measured in pore-volumes-injected (PVI), defined as

$$t_d = \frac{\int_0^t Q_v(t) dt}{\phi_{ave} V} \tag{13}$$

Table 1
Model set-up for the test Cases 4.1–4.2.

Property	4.1	4.2	4.3	4.4
$\mu_w = \mu_{nw}$			1.0	
$K_{rw}^e = K_{rnw}^e$			1.0	
$n_w = n_{nw}$			2.0	
ϕ			0.2	
k_{low}	1.0	10^{-4}	0.01	10^{-5}
k_{high}	1.0	900	100	1.0
L	1.0	10	1.0	1.0
H	0.1	10	0.25	1.0
W	N/A	N/A	0.05	1.0
DOFs $\times 10^4$	0.3, 0.6, 1.2, 2.3, 4.6	1.0, 2.1, 3.8	5.4, 10.3, 19.5, 30.8	5.3, 6.4, 8.5, 10.3

where $Q_v(t)$ is the total volumetric rate at which fluid leaves the model (which is identical here to the rate at which fluid enters the domain given that we model here incompressible flow), φ_{ave} is the volume-weighted arithmetic average porosity of the model and V is the total model volume.

The maximum number of degrees of freedom (DOF) for each numerical simulation are shown in Table 1, where DOF is defined as

$$DOF = N_{CV} + N_{Pres} + N_v, \tag{14}$$

and N_{CV} , N_{Pres} and N_v are the total number of control volumes, pressure finite element nodes and velocity finite element nodes in the numerical domain, respectively. Except where results are benchmarked against analytic or semi-analytic solutions, the grid Courant number is < 1 . This small Courant number ensures that convergence of the non-linear solver does not affect the results.

We demonstrate the method using four models, described in Table 1. Model 1 is 2-D and homogeneous, and allow comparison of numerical results against a semi-analytical solution for 1-D flow. We report here the L_1 and L_2 error norms between the numerical and semi-analytical solutions. Model 2 (2-D), and Models 3 and 4 (3-D) are heterogeneous, and demonstrate the utility of the new method. We compare results obtained using the new discontinuous method with a linear discontinuous pressure approximation and quadratic discontinuous velocity approximation (i.e. the element pair; see Fig. 3) against the conventional continuous CVFE method of [36] with a linear continuous pressure approximation and linear discontinuous velocity approximation (i.e. the element pair) with fixed meshes.

We report the error in terms of the mass fraction leaked into low permeability domains, defined as the volume-weighted average change in the wetting phase saturation from the initial (reference) value within the domain

$$\epsilon_{max} = \frac{\sum_i^{N_l} (S_w - S_{Swirr} \Omega_{CV_i})}{\sum_i^{N_l} \Omega_{CV_i}}, \tag{15}$$

normalized against the largest amount observed in a given suite of experiments (ϵ_{max}). Note that the numerical models are designed such that the mass leakage should be very small over the modelled timescales, so this quantity is a suitable error metric. Here, N_l is the number of CVs within the low permeable region of interest and S_w is the wetting-phase saturation in CV_i , that should remain unchanged. A similar error metric was used by [2].

We characterize computational cost in terms of the number of DOF. Characterizing computational cost in this way avoids any bias introduced by hardware or software and is consistent with [2].

4. Results

4.1. Benchmarking against 2-D Buckley–Leverett solutions

We begin by using a fixed mesh and comparing a pseudo 1D numerical model (Fig. 5) against the analytic Buckley–Leverett (BL) solution ([10]) for the displacement of a non-wetting phase by a wetting phase in a homogeneous domain. Fig. 6 shows a snapshot of the saturation of the displacing fluid along a 1-D profile through the centre of the model, along with the analytical solution and the errors obtained using different numbers of DOFs. Results are shown using the new element pair reported here (P₂DG–P₁DG) and the equivalent conventional element pair with continuous pressure representation (P₁DG–P₁). In this way, the P₂DG–P₁DG is compared against a classical CVFEM in a homogeneous domain. Both element pairs capture the shock front and also the rarefaction (smooth variation in saturation) behind the front. In all cases, the global mass balance errors are $< 10^{-3}$. Moreover, the L_1 - and L_2 -error norms show close-to-linear convergence (Fig. 6(B) and (D)), which is the best that can be expected because flux-limiting of all higher-order methods is required to ensure stability at the shock-front (see [29]).

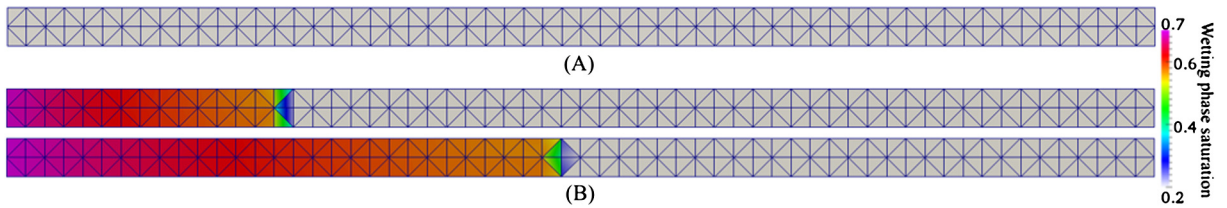


Fig. 5. (A) 2D mesh used in the BL test cases; saturation data for comparison with the 1D analytical solution are obtained along the centre of the domain. The wetting phase is injected over the left-hand face; (B) show the wetting phase saturation for the BL test cases, at $t_d = 0.1$ and $t_d = 0.2$ respectively.

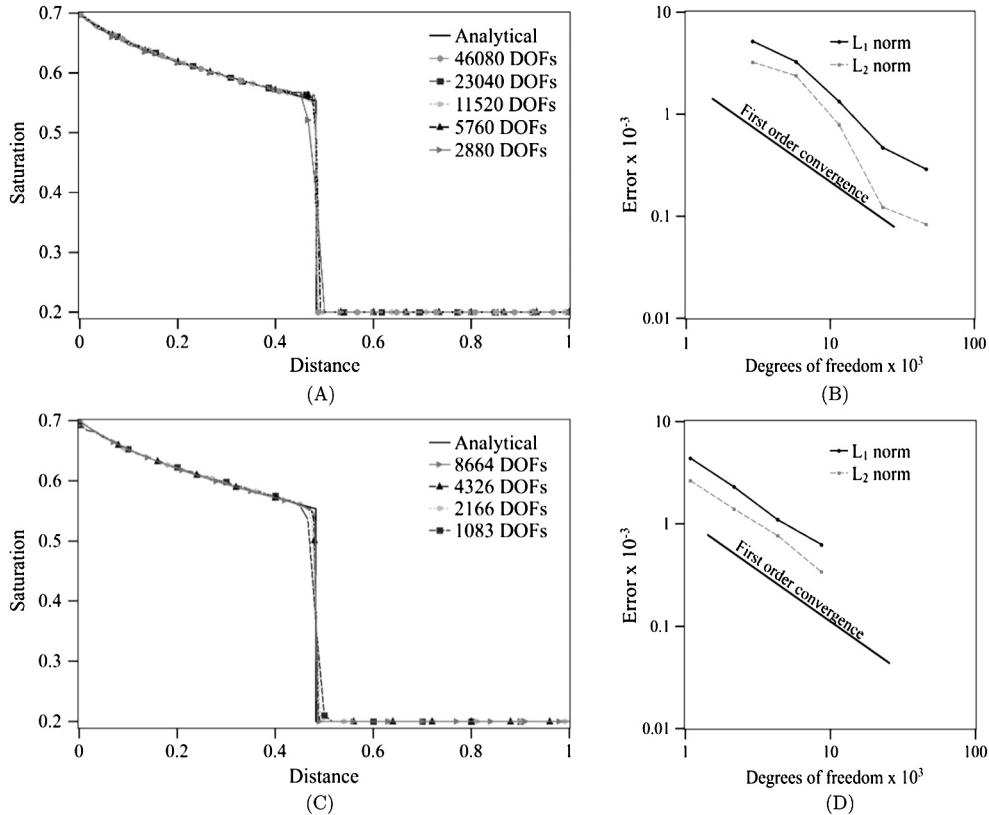


Fig. 6. (A) and (C) Wetting phase saturation as a function of dimensionless distance, comparing the analytic BL solution to the numerical solutions for various 2D simulations using (A) the P_2 DG– P_1 DG element pair with 4 elements in the Y direction and 60, 120, 240, 480 and 960 elements in the X direction (see Fig. 5), totalling 2880, 5760, 11520, 23040 and 46080 DOF respectively, and (C) the P_1 DG– P_1 element pair with 4 elements in the Y direction and 60, 120, 240 and 480 elements in the X direction (see Fig. 5), totalling 1083, 2166, 4326 and 8664 DOF respectively. Solution reported at $t_d = 0.2$. (B) and (D) Error metrics versus the number of DOF using (B) the element pair P_2 DG– P_1 DG and (D) the element pair P_1 DG– P_1 .

Linear convergence is very uncommon in the literature; where reported, most observe convergence of around 0.5 (see, for example, [34], [50], [2]). We have obtained similar results in numerous other test cases (see also [36] using the equivalent CVFEM with continuous pressure). The pressure obtained here using the discontinuous method is very close to that obtained using the continuous method (Fig. 7). Allowing pressure to be discontinuous between elements does not introduce non-physical step-changes in pressure. This comparison is an important rationale for examining such a test case. However, for a case with homogeneous permeability, the classical CVFEM formulation is preferable as it requires fewer DOFs to obtain the same quality of solution (compare Fig. 6(B) and Fig. 6(D)). This is due to the extra-velocity nodes required in the P_2 DG– P_1 DG element pair used to represent the velocity.

4.2. Thin barriers to flow: test case of [20]

We next test the new implementation using a 2-D model developed by [20]. The model contains 4 domains partially separated by low-permeability barriers (Fig. 8(A)). The upper right and bottom left domains have an isotropic dimensionless permeability of 100, and the upper left and bottom right regions have an anisotropic dimensionless permeability which is 900 in the direction bottom-left to top-right, and 100 in the direction orthogonal to this. The low permeability barriers have

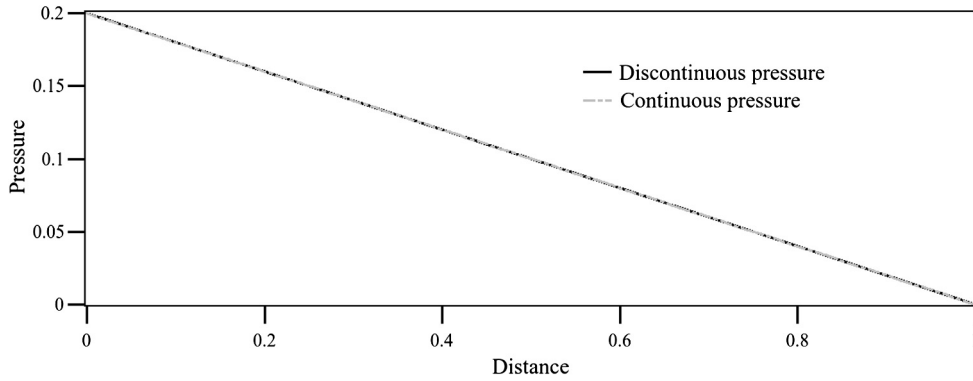


Fig. 7. Pressure vs distance plot for the continuous pressure formulation of [36] and for the discontinuous pressure formulation presented here. The continuous and discontinuous pressure solutions coincide within the plotted line width.

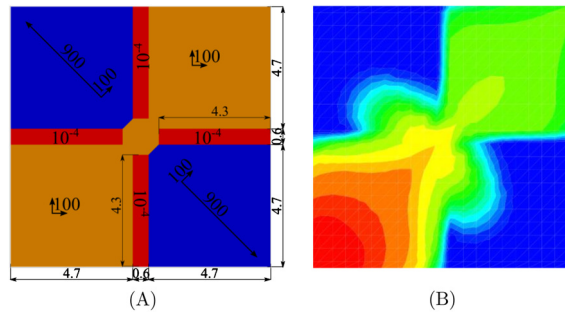


Fig. 8. (A) Permeability of the [20] test model with one-element thick barriers (shown in red). The zones in orange have an isotropic dimensionless permeability of 100; the one-element thick barriers have an isotropic dimensionless permeability of 10^{-4} . The regions in blue have an anisotropic permeability of 900 and 100 oriented as shown. (B) Snapshot of the injected wetting phase saturation obtained by [20] using a conventional CVFE method in which CVs span several FEs. The non-wetting phase is injected through the lower left corner and fluid is extracted from the right top corner. Note how the non-wetting phase is transported through the low-permeable barriers; this is a numerical artifact introduced by the control volumes that span the boundary between the high and low permeability domains. (For interpretation of the references to colour in this figure legend, the reader is referred to the web version of this article.)

an isotropic dimensionless permeability of 10^{-4} . The model was used by [20] to show an endemic problem for conventional CVFE approaches, which transport saturation through permeability barriers that are one element thick regardless of the order of the elements used (Fig. 8(B)). The wetting phase is injected into the domain through the lower left corner and flows towards the top right corner.

We first replicate the results of [20] using the continuous CVFE method presented by [36] and a fixed mesh. Note that this CVFE method mimics numerous classical CVFE methods published in the literature. As expected, the results are similar to those obtained by [20]: mass leakages causes saturation to be erroneously transported through the one-element-thick barriers as a result of the CVs that span domain boundaries (Fig. 9 (A–B)). Maintaining the one-element-thick barriers but refining the mesh elsewhere does not solve the problem and yields only a small decrease in the normalized error (Fig. 10). In contrast, the new discontinuous method reported here preserves the barriers (Fig. 9 (C–D)), even with the same number of DOF as the continuous approach reduces the error by over one order of magnitude (Fig. 10, compare diamonds and circles).

The new discontinuous CVFE method yields significantly smaller error at the same or reduced computational cost compared to conventional continuous methods. Thus our formulation is able to resolve the long-standing problem with conventional CVFE methods identified by [20].

4.3. High permeability fracture in a low permeability domain

Thin, high permeability domains are ubiquitous in many reservoirs and may be stratigraphic, sedimentologic or structural in origin. However, CVFE methods in which CVs span the boundaries between high- and low-permeability domains can introduce significant dispersion of saturation across the domain boundaries, which compromises the accuracy of the numerical solutions unless very small elements are used at the boundaries (e.g. Fig. 2). We test here our new formulation using the example 3-D model of a high permeability ‘fracture’ embedded in a low permeability domain presented by [2] (Fig. 11). The wetting phase flows into the model over one face via a domain of intermediate permeability, passing through a high permeability ‘fracture’ embedded in a low permeability domain, with fluid leaving the model through the opposing

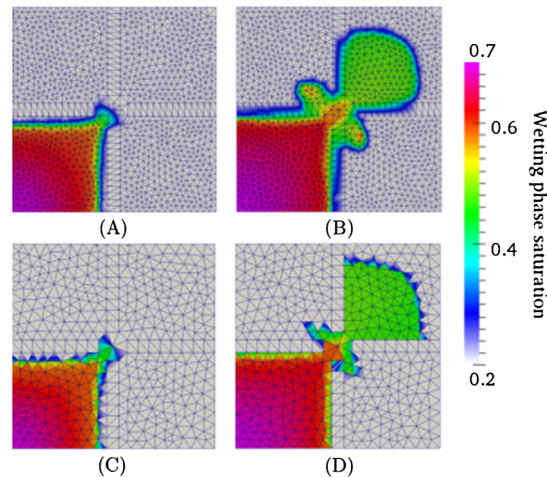


Fig. 9. Wetting phase saturation at $t_d = 0.08$ (plots A, C) and $t_d = 0.15$ (plots B, D) using (A, B) the conventional continuous CVFE method of [36] with 9622 DOF; (E, F) the new discontinuous method with 9648 DOF.

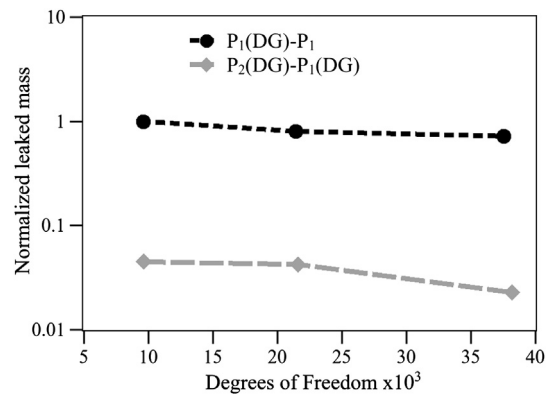


Fig. 10. Normalized mass leaked into the low permeability barriers in the Edwards model at $t_d = 0.15$ for the continuous CVFE method and the new discontinuous method.

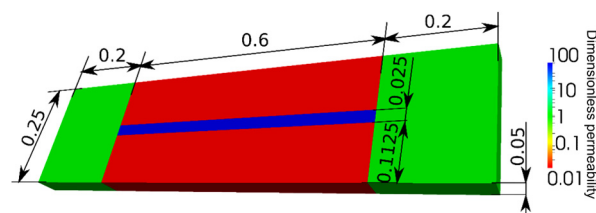


Fig. 11. Permeability map and dimensions of the fracture model (modified from [2]). There is a permeability contrast of 10^4 between the high permeability fracture and the surrounding low permeability domain. The fracture connects two domains of moderate permeability.

face via a second intermediate permeability domain. Visual comparison of the solutions shows that the continuous CVFE method causes significant and non-physical mass leakage of the wetting phase into the low permeability domain surrounding the high permeability ‘fracture’, caused again by the CVs that span the domain boundaries (Fig. 12 (A–B)). The mass leakage results in a large error that is only slightly reduced by increasing the mesh resolution (Fig. 13). The mass leakage also causes flow of the wetting phase in the fracture to be significantly retarded (Fig. 12 (A–B)).

The new discontinuous formulation reported here effectively retains the wetting phase within the high permeability layer (Fig. 12 (C–D)), yielding a significant reduction in the error (Fig. 13) and leading to much earlier arrival of the wetting phase at the outlet face of the model (Fig. 12). The new method yields an increase in solution accuracy of almost two orders of magnitude compared to the continuous CVFE method, despite the conventional method employing almost an order of magnitude more DOF (compare far right circle with the far left diamond in Fig. 13).

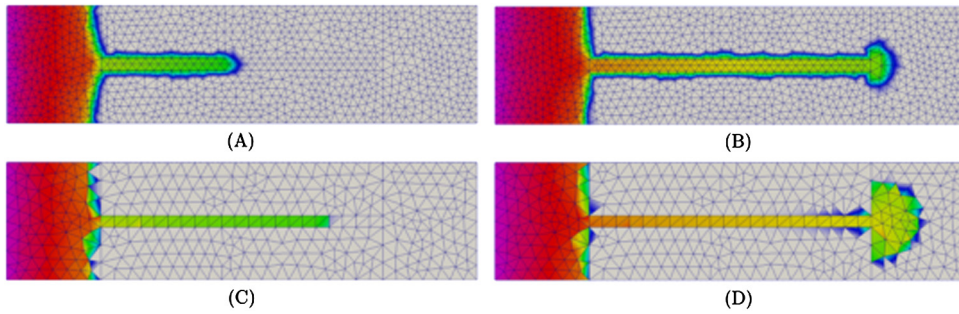


Fig. 12. 2D section through the centre of the fracture model showing the wetting phase saturation at $t_d = 0.02$ (plots A, C) and $t_d = 0.0266$ (plots B, D) using (A, B) the continuous CVFE method and a fixed mesh with 53192 DOF; (C, D) and the new discontinuous method with 55350 DOF.

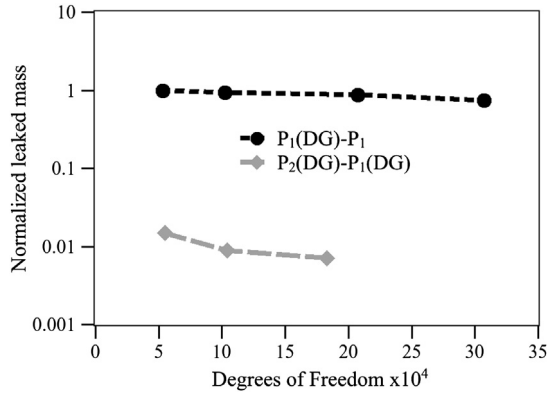


Fig. 13. Normalized mass leaked into the low permeability region in the fracture model at $t_d = 0.02$ for the continuous CVFE method and the new discontinuous method.

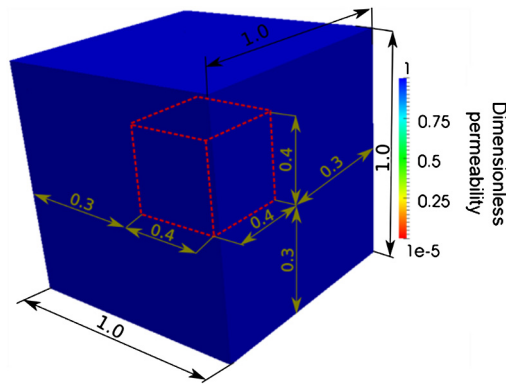


Fig. 14. Permeability map and dimensions of the barrier model. There is a permeability contrast of 10^5 between the cubic barrier at the centre of the model and the surrounding domain.

4.4. Barrier to flow embedded in a 3D domain

We finish by simulating flow of the wetting phase into a cubic domain containing a low permeability cubic barrier (permeability contrast of 10^5) (Fig. 14). The wetting phase is injected over one face of the domain and fluid is produced over the opposite face. Fig. 15 shows the wetting phase along 2D slices through the centre of the 3-D domain that span the inlet and outlet boundaries. The wetting phase is injected over the left-hand face in these images. The continuous method results in mass leakage into the barrier (Fig. 15(A–B)) which is again not significantly reduced by mesh refinement (Fig. 16). In contrast, the new discontinuous formulation properly preserves the barrier (Fig. 15(C–D)), yielding a one order of magnitude reduction in error compared to the continuous method (Fig. 16). Note that the small increase in error with increasing mesh resolution is an artefact introduced by the unstructured mesh geometry in this particular example. Thus the new discontinuous CVFE formulation is able to improve solution quality, measured by a variety of metrics, compared to a conventional continuous CVFE method and at lower computational cost.

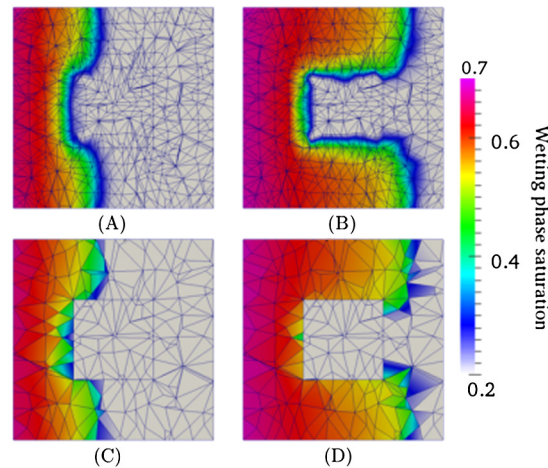


Fig. 15. 2D section through the centre of the barrier model showing the wetting phase saturation at $t_d = 0.32$ (plots A, C) and $t_d = 0.64$ (plots B, D) using (A, B) the continuous CVFE method and a mesh with 103232 DOF; (C, D) the new discontinuous method and a mesh with 52632 DOF.

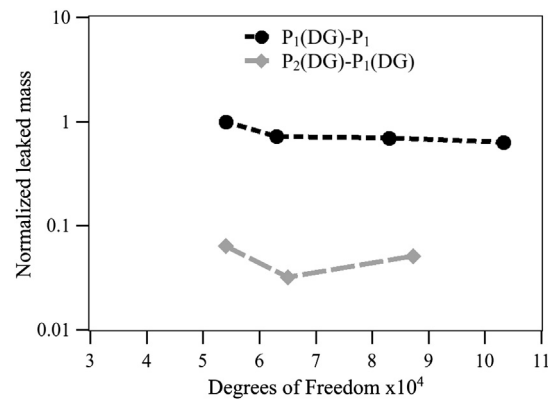


Fig. 16. Normalized mass leaked into the low permeability region in the barrier model at $t_d = 0.32$ for the continuous CVFE method and the new discontinuous method.

5. Conclusions

A new, high-order, control-volume-finite-element (CVFE) method is presented that can capture sharp saturation changes at material property boundaries within 3D models of heterogeneous reservoirs. The method has discontinuous N th-order representation for pressure and $(N + 1)$ th-order representation for velocity and is mass conservative. Unlike conventional CVFE formulations, it does not require the use of control volumes that span domain boundaries. We demonstrate that the approach, amongst other features, accurately preserves sharp saturation changes associated with geologic features with contrasting permeability, allowing efficient simulation of flow in highly heterogeneous models. Moreover, accurate solutions are obtained at significantly lower computational cost than an equivalent fine, fixed mesh and conventional CVFE methods. We present a solution for a long-standing problem associated with the use of classical CVFE methods to model flow in highly heterogeneous porous media. Although we focus here on the common case of permeability heterogeneity, the method may also be applicable to capillary heterogeneity.

Acknowledgements

Funding for Salinas from ExxonMobil is gratefully acknowledged. Pavlidis would like to acknowledge the support from: EPSRC “Reactor Core-Structure Relocation Modelling for Severe Nuclear Accident” (EP/M012794/1) and Horizon 2020 “In-Vessel Melt Retention” (662157). Xie is supported by EPSRC (“Multi-Scale Exploration of Multiphase Physics in Flows” – MEMPHIS, EP/K003976/1). Part funding for Jackson under the TOTAL Chairs programme at Imperial College is also acknowledged. No data was generated in the course of this work. For further information, please contact the corresponding author at (pablo.salinas@imperial.ac.uk), the AMCG Group (www.imperial.ac.uk/earth-science/research/research-groups/amcg/) or the NORMS group (www.imperial.ac.uk/earth-science/research/research-groups/norms) as required.

References

- [1] I. Aavatsmark, An introduction to multipoint flux approximations for quadrilateral grids, *Comput. Geosci.* 6 (2002) 405–432, <http://dx.doi.org/10.1023/A:1021291114475>.
- [2] A. Abushaikha, M. Blunt, O. Gosselin, C. Pain, M.D. Jackson, Interface control volume finite element method for modelling multi-phase fluid flow in highly heterogeneous and fractured reservoirs, *J. Comput. Phys.* (2015) 41–61, <http://dx.doi.org/10.1016/j.jcp.2015.05.024>.
- [3] D.G. Anderson, Iterative procedures for nonlinear integral equations, *J. Assoc. Comput. Mach.* 12 (1965) 547–560.
- [4] K. Aziz, A. Settari, *Petroleum Reservoir Simulation*, Applied Science Publishers, London, 1979.
- [5] P. Bastian, R. Helmig, Efficient fully-coupled solution techniques for two-phase flow in porous media. parallel multigrid solution and large scale computations, *Adv. Water Resour.* 23 (1998) 199–216.
- [6] B. Batista Fernandes, F. Marcondes, K. Sepehrnoori, Investigation of several interpolation functions for unstructured meshes in conjunction with compositional reservoir simulation, *Numer. Heat Transf., Part A, Appl.* 64 (2013) 974–993, <http://dx.doi.org/10.1080/10407782.2013.812006>.
- [7] S. Bazr-Afkan, S. Matthai, A new hybrid simulation method for multiphase flow on unstructured grids with discrete representation of material interfaces, *MIAMG* (2011) 294–305.
- [8] M. Belayneh, M. Geiger, S. Matthai, Numerical simulation of water injection into layered fractured carbonate reservoir analogs, *Am. Assoc. Pet. Geol. Bull.* 90 (2006) 1473–1493.
- [9] M. Blunt, B. Rubin, Implicit flux limiting schemes for petroleum reservoir simulation, *J. Comput. Phys.* (1992) 194–210.
- [10] S. Buckley, M. Leverett, Mechanism of fluid displacements in sands, *Trans. AIME* (1942) 107–116.
- [11] V. Dalen, Simplified finite-element models for reservoir flow problems, *Soc. Pet. Eng. J.* (1979) 333–343.
- [12] P. Deveugle, M.D. Jackson, G. Hampson, M. Farrell, A. Sprague, J. Stewart, C. Calvert, Characterization of stratigraphic architecture and its impact on fluid flow in a fluvial-dominated deltaic reservoir analog: upper Cretaceous Ferron Sandstone member, Utah, *Am. Assoc. Pet. Geol. Bull.* 95 (2011) 693–727, <http://dx.doi.org/10.1306/09271010025>.
- [13] J. Douglas, Finite difference methods for two-phase incompressible flow in porous media, *SIAM J. Numer. Anal.* 20 (1983) 681–696, <http://dx.doi.org/10.1137/0720046>.
- [14] C.J. van Duijn, X. Cao, I.S. Pop, Two-phase flow in porous media: dynamic capillarity and heterogeneous media, *Comput. Geosci.* 114 (2016) 283–308, <http://dx.doi.org/10.1007/s11242-015-0547-0>.
- [15] C.J. van Duijn, J. Molenaar, M. de Neef, The effect of capillary forces on immiscible two-phase flow in heterogeneous porous media, *Transp. Porous Media* 21 (1995) 71–93.
- [16] C.J. van Duijn, M. de Neef, Similarity solution for capillary redistribution of two phases in a porous medium with a single discontinuity, *Adv. Water Resour.* 21 (1998) 451–461.
- [17] L. Durlafsky, A triangle based mixed finite element finite volume technique for modelling two-phase flow through porous media, *J. Comput. Phys.* 105 (1993) 252–266.
- [18] L. Durlafsky, Accuracy of mixed and control volume finite element approximations to Darcy velocity and related quantities, *Water Resour. Res.* 30 (1994) 965–973.
- [19] M. Edwards, Unstructured, control-volume distributed, full-tensor finite-volume schemes with flow based grids, *Comput. Geosci.* 6 (2002) 433–452.
- [20] M. Edwards, Higher-resolution hyperbolic-coupled-elliptic flux-continuous cvd schemes on structured and unstructured grids in 2-d, *Int. J. Numer. Methods Fluids* 51 (2006) 1059–1077.
- [21] M. Edwards, Higher-resolution hyperbolic-coupled-elliptic flux-continuous cvd schemes on structured and unstructured grids in 3-d, *Int. J. Numer. Methods Fluids* 51 (2006) 1079–1095.
- [22] P. Forsyth, A control volume finite element approach to NAPL groundwater contamination, *SIAM J. Sci. Stat. Comput.* 12 (1991) 1029–1057.
- [23] L. Fung, A. Hiebert, L. Nghiem, Reservoir simulation with control-volume finite element method, *SPE Reserv. Eng.* 7 (1992) 349–357.
- [24] S. Geiger, S. Roberts, S. Matthai, C. Zoppou, A. Burri, Combining finite element and finite volume methods for efficient multiphase flow simulations in highly heterogeneous and structurally complex geologic media, *Geofluids* 4 (2004) 284–299.
- [25] J. Gomes, C. Pain, M.D. Eaton, M.D. Piggott, A. Goddard, A. Ziver, Y. Yamane, Modelling of criticality within a MOX powder system – coupled neutronics and thermofluids dynamics model, *Ann. Nucl. Energy* 35 (2008) 2073–2092.
- [26] J. Gomes, D. Pavlidis, P. Salinas, Z. Xie, J. Percival, Y. Melnikova, C. Pain, M.D. Jackson, A force-balanced control volume finite element method for multiphase porous media flow modelling, *Int. J. Numer. Methods Fluids* (2016), <http://dx.doi.org/10.1002/flid.4275>.
- [27] G. Graham, M.D. Jackson, G. Hampson, Three-dimensional modeling of clinofolds in shallow-marine reservoirs: Part 1. Concepts and application, in: *AAPG Bulletin*, 2015, pp. 1013–1047.
- [28] D. Gunasekera, J. Cox, P. Lindsey, The generation and application of k-orthogonal grid systems, in: *SPE Reservoir Simulation Symposium*, 1997.
- [29] A. Harten, J. Hyman, P. Lax, On finite-difference approximations and entropy conditions for shocks, *Commun. Pure Appl. Math.* (1976) 297–322.
- [30] R. Helmig, H. Huber, Comparison of Galerkin-type discretization techniques for two-phase flow in heterogeneous porous media, *Adv. Water Resour.* 21 (1998) 697–711.
- [31] R. Helmig, A. Weiss, B.I. Wohlmuth, Dynamic capillary effects in heterogeneous porous media, *Comput. Geosci.* 11 (2007) 261–274, <http://dx.doi.org/10.1007/s10596-007-9050-1>.
- [32] R. Helmig, A. Weiss, B.I. Wohlmuth, Variational inequalities for modeling flow in heterogeneous porous media with entry pressure, *Comput. Geosci.* 13 (2009) 373, <http://dx.doi.org/10.1007/s10596-008-9125-7>.
- [33] H. Hoteit, A. Firoozabadi, Compositional modeling by the combined discontinuous Galerkin and mixed methods, *SPE J.* 11 (2006) 19–34.
- [34] H. Hoteit, A. Firoozabadi, Numerical modeling of two-phase flow in heterogeneous permeable media with different capillarity pressures, *Adv. Water Resour.* 31 (2008) 56–73, <http://dx.doi.org/10.1016/j.advwatres.2007.06.006>.
- [35] P. Huyakorn, G. Pinder, A new finite element technique for the solution of two-phase flow through porous media, *Adv. Water Resour.* (1978) 285–298.
- [36] M.D. Jackson, J. Percival, P. Mostaghimi, B. Tollit, D. Pavlidis, C. Pain, J. Gomes, A. El-Sheikh, P. Salinas, A. Muggeridge, M. Blunt, Reservoir modeling for flow simulation by use of surfaces, adaptive unstructured meshes, and an overlapping-control-volume finite-element method, *SPE Reserv. Eval. Eng.* 18 (2015), <http://dx.doi.org/10.2118/163633-PA>.
- [37] P. Jenny, H. Tchelepi, S. Lee, Unconditionally convergent nonlinear solver for hyperbolic conservation laws with s-shaped flux functions, *J. Comput. Phys.* 228 (2009) 7497–7512.
- [38] B. Legler, H.D. Johnson, G.J. Hampson, B. Massart, C.L. Jackson, M.D. Jackson, A. El-Barkooky, R. Ravnas, Facies model of a fine-grained, tide-dominated delta: lower Dir Abu Lifa member (Eocene), Western Desert, Egypt, *Sedimentology* 60 (2013) 1313–1356, <http://dx.doi.org/10.1111/sed.12037>.
- [39] S. Matringe, R. Juanes, H. Tchelepi, Mixed finite element and related control volume discretizations for reservoir simulation on three-dimensional unstructured grids, in: *SPE Reservoir Simulation Symposium*, 26–28 February, Houston, Texas, USA, SPE, 2007, SPE paper 106117.
- [40] S. Matthai, A. Mezentsev, M. Belayneh, Finite element-node centred finite-volume two-phase flow experiments with fractured rock represented by unstructured hybrid element meshes, *SPE Reservoir Evaluation and Engineering* (2007) 93341.
- [41] M. Mlacnik, L. Durlafsky, Z. Heinemann, Sequentially adapted flow-based PEBI grids for reservoir simulation, *SPE J.* (2006) 317–327, <http://dx.doi.org/10.2118/90009-PA>.

- [42] J. Moortgat, A. Firoozabadi, Mixed-hybrid and vertex-discontinuous-Galerkin finite element modeling of multiphase compositional flow on 3D unstructured grids, *J. Comput. Phys.* 315 (2016) 476–500, <http://dx.doi.org/10.1016/j.jcp.2016.03.054>.
- [43] P. Mostaghimi, J. Percival, D. Pavlidis, R. Ferrier, J. Gomes, G. Gorman, M.D. Jackson, S. Neethling, C. Pain, Anisotropic mesh adaptivity and control volume finite element methods for numerical simulation of multiphase flow in porous media, *Math. Geosci.* 347 (2015) 673–676, <http://dx.doi.org/10.1007/s11004-014-9579-1>.
- [44] H. Nick, S. Matthai, A hybrid finite-element finite-volume method with embedded discontinuities for solute transport in heterogeneous media, *Vadose Zone J.* 10 (2011) 299–312.
- [45] J.M. Nordbotten, I. Aavatsmark, G.T. Eigestad, Monotonicity of control volume methods, *Numer. Math.* 106 (2007) 255–288, <http://dx.doi.org/10.1007/s00211-006-0060-z>.
- [46] M. Pal, M.G. Edwards, q-families of cvd(mpfa) schemes on general elements: numerical convergence and the maximum principle, *Arch. Comput. Methods Eng.* 17 (2010) 137–189.
- [47] D.W. Peaceman (Ed.), *Fundamentals of Numerical Reservoir Simulation*, Elsevier, 1977.
- [48] P. Salinas, D. Pavlidis, Z. Xie, A. Adam, C.C. Pain, M.D. Jackson, Improving the convergence behaviour of a fixed-point-iteration solver for multiphase flow in porous media, *Int. J. Numer. Methods Fluids* (2016), <http://dx.doi.org/10.1002/flid.4357>.
- [49] P. Salinas, D. Pavlidis, Z. Xie, C. Jacquemyn, Y. Melnikova, C.C. Pain, M.D. Jackson, Improving the robustness of the control volume finite element method with application to multiphase porous media flow, *Int. J. Numer. Methods Fluids* (2017) 1–12, <http://dx.doi.org/10.1002/flid.4381>.
- [50] K. Schmid, S. Geiger, K. Sorbie, Higher order FE-FV method on unstructured grids for transport and two-phase flow with variable viscosity in heterogeneous porous media, *J. Comput. Phys.* 241 (2013) 416–444, <http://dx.doi.org/10.1016/j.jcp.2012.12.017>.
- [51] H. Sterck, P. Ullrich, *Introduction to Computational Mathematics*, University of Waterloo, 2006.
- [52] K. Su, J.P. Latham, D. Pavlidis, J. Xiang, F. Fang, P. Mostaghimi, J.R. Percival, C.C. Pain, M.D. Jackson, Multiphase flow simulation through porous media with explicitly resolved fractures, *Geofluids* (2015), <http://dx.doi.org/10.1111/gfl.12129>.
- [53] M. Wheeler, I. Yotov, A multipoint flux mixed finite element method, *SIAM J. Numer. Anal.* 44 (2006) 2082–2106.
- [54] X.H. Wu, R. Parashkevov, Effect of grid deviation on flow solutions, *SPE J.* (2009) 67–77, <http://dx.doi.org/10.2118/92868-PA>.
- [55] Z. Xie, D. Pavlidis, P. Salinas, J. Percival, C. Pain, O. Matar, A balanced-force control volume finite element method for interfacial flows with surface tension using adaptive anisotropic unstructured meshes, *Comput. Fluids* 138 (2016) 38–50, <http://dx.doi.org/10.1016/j.compfluid.2016.08.005>.
- [56] A. Younes, M. Fahs, B. Belfort, Monotonicity of the cell-centred triangular {MPFA} method for saturated and unsaturated flow in heterogeneous porous media, *J. Hydrol.* 504 (2013) 132–141, <http://dx.doi.org/10.1016/j.jhydrol.2013.09.041>.